EFFECT OF FLOW IRREGULARITY ON OSCILLATORY BOUNDARY LAYER FLOW

M. Bhawanin[1], T.O'Donoghue[1], D. A. van der A[1] and J.S. Ribberink[2]

The paper reports on new oscillatory flow tunnel experiments in which detailed measurements have been made of boundary layer velocities for full-scale regular and irregular oscillatory flows over sand-rough and gravel-rough fixed beds. The irregular flows were generated by amplitude modulation of the corresponding regular flows, to give same free-stream u_{rms} and same velocity and acceleration skewness. The experimental setup is described and initial results relating to flow structure, turbulence and bed shear stress are presented. Results presented for boundary layer development, turbulence intensity, turbulent stress and log-law-based estimates of bed shear stress suggest that the hydrodynamics within a flow half-cycle are largely independent of the previous flow half-cycle, at least close to the bed where the presented results have focused. Time-history effects are not entirely absent however, especially higher up from the bed. More detailed analysis is needed to elucidate further.

Keywords: oscillatory flow; boundary layer; turbulence; flow tunnel; laboratory experiments.

INTRODUCTION

Understanding sediment dynamics under waves requires knowledge of the hydrodynamics within the bottom boundary layer generated by the wave-induced near-bed oscillatory fluid motions. Previous large-scale laboratory experiments by Sleath (1987), Jensen et al. (1989), van der A et al. (2011) and Yuan and Madsen (2014) have produced valuable insights and data for boundary layer hydrodynamics for regular oscillatory flow conditions. However, waves in the field are irregular and the irregularity may play a significant role in the near-bed hydro- and sediment dynamics through unsteady, time-history effects. To the authors' knowledge, previous laboratory experiments involving detailed measurements of velocities within the bottom boundary layer under irregular waves and oscillatory flows are limited to the small-scale wave experiments of Klopman (1994) and the wind-tunnel experiments of Tanaka and Samad (2006).

The present paper reports on new experiments in which detailed measurements are made of boundary layer velocities for full-scale oscillatory flows with varying irregularity. The experiments were conducted over fixed (immobile), rough beds, yielding measurements of the time-varying boundary layer structure, turbulence and shear stress. Here we present an overview of the experiments and initial results relating to key aspects of the irregular oscillatory boundary layer flow.

EXPERIMENTAL SETUP

The experiments were conducted in the Aberdeen Oscillatory Flow Tunnel (AOFT), a large facility capable of generating "full-scale" oscillatory flows, with flow period typically in the range 4-10s and flow amplitude up to 1.5m. The AOFT has an overall length of 16m, with a 10m-long rectangular test section, 0.75 m high and 0.3 m wide (Figure 1). For the present experiments the test bed was 6m long and consisted of 25 mm-thick PVC mounted on a rigid, stainless steel frame. Measurements were obtained over two bed roughness conditions: coarse sand with d_{50} = 0.46 mm and gravel with d_{50} = 6 mm. For the coarse sand, a thin sheet of adhesive-backed plastic was bonded to the PVC panels and the sand was then bonded to the plastic using marine varnish. For the gravel experiments, a 2 mm thick stainless steel sheet was fixed to the PVC panels and the sediment was then bonded directly to the sheets using marine varnish.

[1] School of Engineering, University of Aberdeen, Aberdeen AB24 3UE, Scotland. m.bhawanin@abdn.ac.uk, t.odonoghue@abdn.ac.uk, d.a.vandera@abdn.ac.uk

[2] Faculty of Engineering, University of Twente, PO Box 217, 7500 AE Enschede, the Netherlands. j.s.ribberink@utwente.nl

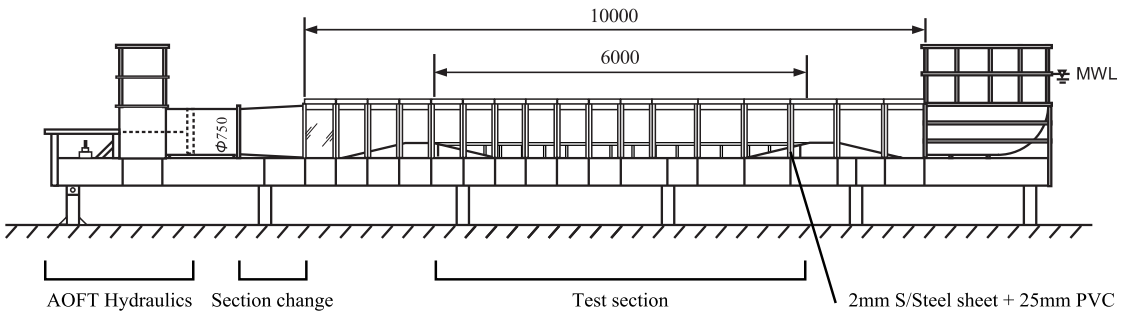

Figure 1. Aberdeen Oscillatory Flow Tunnel (AOFT) set up for fixed bed experiments

Flow Conditions

Experiments were conducted for a range of regular and corresponding irregular oscillatory flow conditions. The regular flows, $u_{reg}(t)$, were specified by wave period, T, rms free-stream velocity, u_{rms}, degree of velocity skewness, u_{sk}, and degree of acceleration skewness, a_{sk}. The corresponding irregular flows, $u_{irr}(t)$, were obtained by amplitude modulation of the regular flows via

$$u_{irr}\left(t\right) = M_1\left\{1 + M_2 \frac{\arctan\left(\dfrac{b\sin\left(\omega_g t\right)}{1-b\cos\left(\omega_g t\right)}\right)}{\arctan\left[b\left(1-b^2\right)^{-0.5}\right]}\right\} u_{reg}\left(t\right) \qquad (1)$$

where $\omega_g = 2\pi/T_g$ is the group radial frequency; M_2 $(0 \le M_2 \le 1)$ determines the strength of the modulation; multiplier M_1 is used to achieve the desired u_{rms} for the modulated signal; b determines the shape of the modulation: $b<0$, $b=0$ and $b>0$ produces a backward-leaning-sawtooth, sinusoidal and forward-leaning-sawtooth modulation respectively. For these experiments the regular flow period was set at T = 6s; the modulation period was $T_g = 10T$ and M_1 was set to give same u_{rms} for corresponding regular and irregular flows. The velocity and acceleration skewness, u_{sk}, and a_{sk} respectively is calculated from

$$x_{sk} = \frac{\sum_{i=1}^{N}(x(i)-\overline{x})^3}{\left(\sum_{i=1}(x(i)-\overline{x})^2\right)^{3/2}} \qquad (2)$$

where x = horizontal velocity u or horizontal acceleration a in the free-stream, and the overbar denotes time-average. Corresponding regular and irregular flows have the same skewness; note however that the skewness of individual flow cycles within the irregular group may differ slightly from the skewness of the regular flow.

Figure 2 presents examples of the type of regular/irregular flows synthesised via equation (1). It is appreciated that irregular flows of the type produced here differ substantially from near-bed oscillatory flows generated under irregular waves, but the approach enables isolation of the effect of variation in flow amplitude on the hydrodynamics, keeping all other key parameters constant.

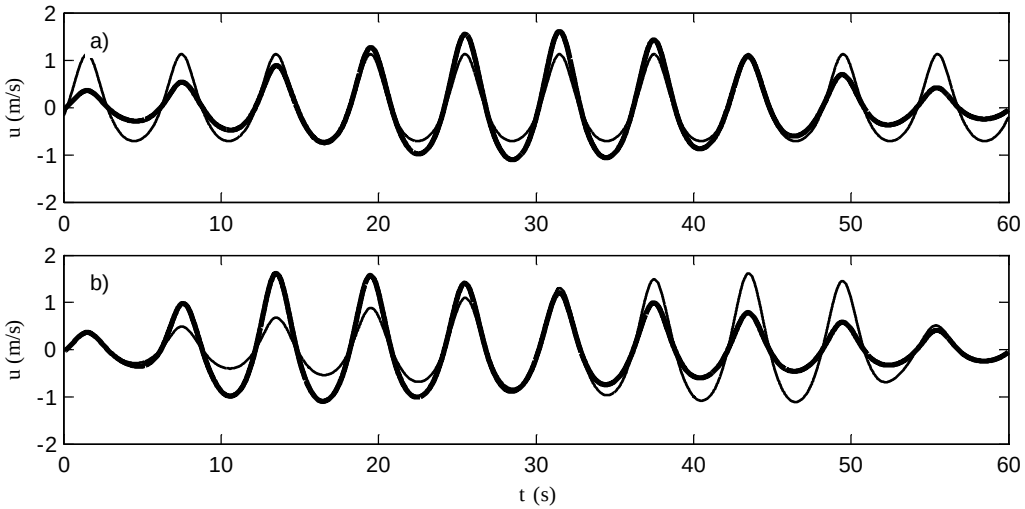

Figure 2. Example specified flow conditions. (a) Regular, velocity-skewed flow (thin line) and corresponding irregular, sine-modulated flow (thick line). (b) Forward-sawtooth (thick line) and backward-sawtooth (thin line) irregular flows corresponding to (a).

Table 1 summarises the test conditions. For the sand-rough bed, experiments were conducted for 3 regular flows – sinusoidal, velocity-skewed, acceleration-skewed – and 5 corresponding irregular flows comprising sine-modulation of the 3 regular flows and forward-sawtooth and backward-sawtooth modulation of the regular velocity-skewed flow. For the gravel-rough bed, experiments were conducted for 2 flows: a regular-velocity-skewed flow and the corresponding sine-modulated irregular flow. The following code is used to distinguish experiments: letters on left, CS/GV denote sand/gravel bed; first letter on right, S/V/A denotes sinusoidal/velocity-skewed/acceleration skewed flow; second letter on right R/I denotes regular/irregular flow; third letter on right S/F/B denotes modulation type for irregular flow, sinusoidal, forward-leaning, backward-leaning.

Table 1. Summary of test conditions.

Exp.	d_{50} (mm)	Reg (R) or Irreg (I)	T (s)	T_g (s)	u_{rms} (m/s)	u_{max} (m/s)	u_{min} (m/s)	u_{sk}	a_{sk}
CS-SR	0.46	R	6	6	0.690	0.940	-0.963	0	0
CS-SIS	0.46	I	6	60	0.680	1.529	-1.583	0	0
CS-VR	0.46	R	6	6	0.564	0.959	-0.614	0.42	0
CS-VIS	0.46	I	6	60	0.567	1.406	-0.982	0.43	0
CS-VIF	0.46	I	6	60	0.565	1.404	-0.989	0.44	0
CS-VIB	0.46	I	6	60	0.568	1.412	-0.989	0.43	0
CS-AR	0.46	R	6	6	0.563	0.776	-0.779	0	1.11
CS-AIS	0.46	I	6	60	0.565	1.288	-1.288	0	1.13
GV-VR	6.00	R	6	6	0.564	0.959	-0.614	0.42	0
GV-VIS	6.00	I	6	60	0.567	1.406	-0.982	0.43	0

Velocity Measurements

Simultaneous horizontal and vertical velocities were measured using a Dantec FiberFlow 2D LDA system, comprising a 300 mW Argon-ion laser and a P60 Burst Spectrum Analyser. The probe is mounted on a computer-controlled traverse with 0.6m range of motion in the x, y and z directions and resolution of 50μm. The LDA provides a point measurement of velocity with a measurement volume 76μm in diameter and 1.2mm deep (transverse to main flow direction). The system was run in "burst" mode with velocity-dependent data capture rates in the range of 600Hz at peak flow velocity; close to the bed, where velocities are lower, data rates of 50 - 150Hz are more typical. The seeding material used was ~5μm PA-12 polyamide nylon particles with specific gravity 1.01. Velocity measurements were made at 40 elevations above the bed, with near logarithmic spacing between positions. The lowest measurement is at 50±25μm above the crest of a locally prominent grain to ensure the laser beams are

not blocked (in what follows, $z = 0$ corresponds to the crest of the grain over which the measurements were made). For the sand-rough bed, velocities were measured along a single vertical line above the bed. In order to account for the bed non-uniformity in the case of the gravel-rough bed, velocities were measured at 40 elevations along one vertical line and at fewer elevations, concentrated in the near-bed region, along nine lines spaced horizontally by 1mm.

Velocities were measured over approximately 50 flow cycles in the case of the regular flows and over 50 flow groups (500 flow cycles) in the case of the irregular flows. For the results presented in the here, the measured velocities were phase-averaged on a 1/15Hz basis: the data were collected into 1/15-Hz bins and data within each bin were de-spiked based on ±6 standard deviations from the mean of the data in the bin. The phase-averaged velocity for the bin is then taken as the weighted average of the (de-spiked) data, where the weighting is based on particle transit time across the measurement volume.

RESULTS

In the following, we present initial results relating to key aspects of the flow including boundary layer development, turbulence intensities and stresses, and bed shear stress.

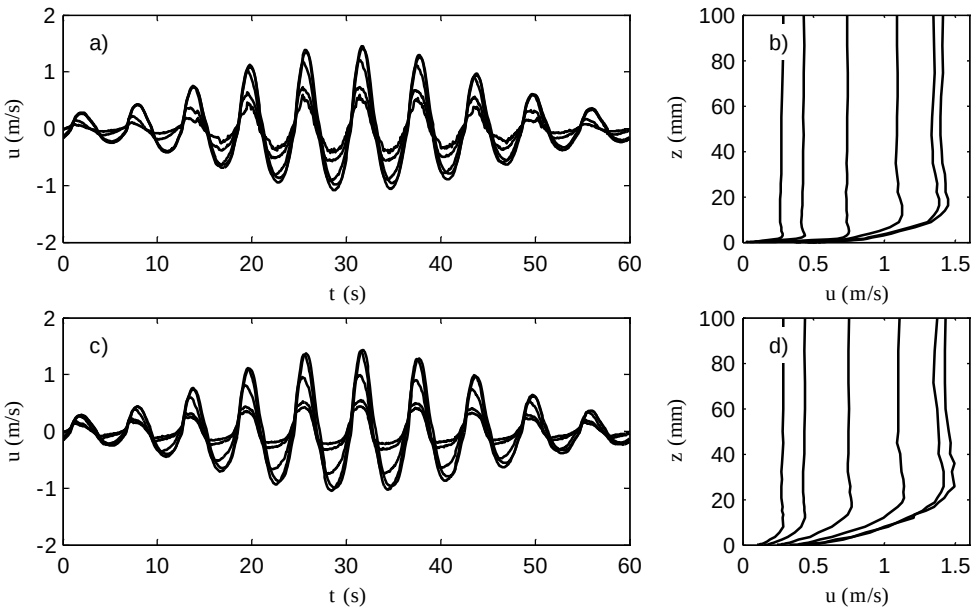

Figure 4. (a) u(t) at z = 0.12, 0.5, 5.05, 16.29 and 101 mm for CS-VIS and (b) u(z) at times of peak positive free-stream velocity for first 6 cycles. (c) u(t) at z =0.1, 0.51, 5.44, 16.68 and 102 mm for GV-VIS and (d) u(z) at times of peak positive velocity for first 6 cycles.

Phase-averaged velocities

Figure 4 shows example time-series and vertical profiles of horizontal velocity for the sand-rough (top) and gravel-rough (bottom) beds for the sine-modulated velocity-skewed flow (VIS). These measurements for irregular flow show similar oscillatory boundary layer flow characteristics seen in previous (and present) regular flow experiments (Sleath, 1987; Jensen et al. 1989; van der A et al. 2011; Yuan and Madsen, 2014): the flow near the bed leads the free-stream flow and the velocity profile within the boundary layer overshoots the free-stream velocity. As expected, the velocity profiles show increasing boundary layer thickness with increasing peak velocity and the higher roughness gravel bed results in a boundary layer thickness that is approximately twice that of the sand-rough bed.

The development of the boundary layer within the irregular flows is illustrated in Figure 5. Here we take a measure of the instantaneous boundary layer thickness as the elevation above the bed where the velocity defect reaches 5% of the instantaneous free-stream velocity. In general, there are two measures of the boundary layer thickness at any particular time: the “inner measure”, indicated by the red markers in Figure 5, corresponds to the first position above the bed where the defect reaches 5% of the instantaneous free-stream velocity; the “outer measure”, indicated by the black markers, corresponds to the first position below the free-stream where the defect reaches 5%. The results show excellent consistency from half-cycle to half-cycle and between the two bed types. As expected, boundary layer

thickness is seen to be much greater in the case of the gravel-rough bed. The red markers show the growth of a new boundary layer soon after flow reversal, which grows throughout the half-cycle until the following flow reversal. The underlying velocity skewness is echoed in the "inner layer" development in that the boundary layer grows faster and deeper during the higher-velocity positive flow half-cycles compared to the negative flow half-cycles. There is also a consistent difference in the behaviour of the outer measure between positive and negative flow cycles: the outer measure is present throughout the whole of the negative half-cycle and peaks strongly at the negative-positive flow reversal, while the outer measure is only present during the accelerating phase of the positive half-cycle. The outer measure shows a distinct time-history effect, especially for the sand-rough bed, with the thickness peaking at approximately 80mm around the 7th flow cycle. The time-history effect is less pronounced in the case of the gravel-rough bed, for which maximum boundary layer thickness is approximately 130mm.

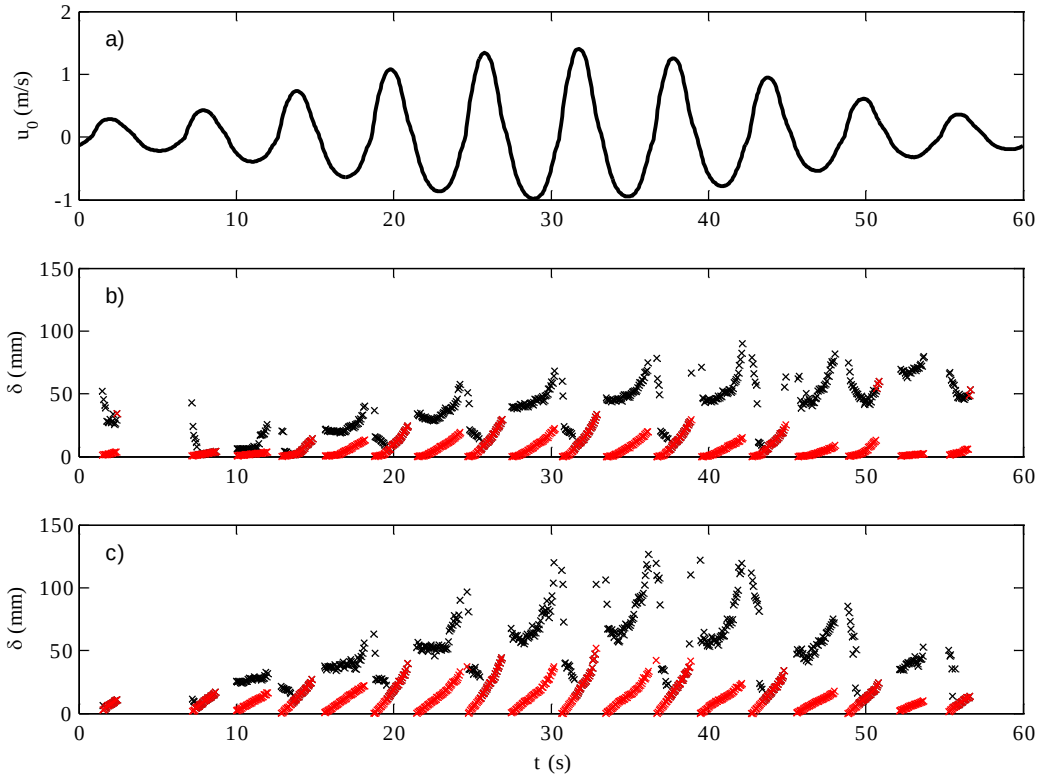

Figure 5. a) Free-stream velocity. b) Boundary layer development for CS-VIS, red markers indicate the "inner measure" and black markers indicate the "outer measure". (c) as (b) but for GV-VIS.

Turbulence intensity

Horizontal flow turbulence intensity, u'_{rms}, is estimated using the root-mean-square of the turbulent fluctuations, i.e.

$$u'_{rms} = \sqrt{\sum_{i=1}^{N} \frac{TT(i)}{\sum TT} \left(u(i) - \tilde{u}\right)^2} \qquad (3)$$

where $u(i)$ is an individual velocity measurement within a phase-bin, N is the number of velocity measurements within the bin, and $\tilde{u}$ is the phase-averaged velocity. The averaging is weighted by particle transit time, TT, of the particle through the measurement volume.

Figure 6 presents contour plots of $u'_{rms}(z,t)$ for two flow conditions over the sand-rough bed: the velocity-skewed regular flow (VR) and the corresponding sine-modulated flow (VIS). The figure also shows the vertical profile of time-averaged horizontal turbulent intensity, $\overline{u'}_{rms}(z)$, the free-stream

horizontal velocity, $u_o(t)$, and $u'_{rms}(t)$ at elevation *z* corresponding to the peak in the vertical profile of $\overline{u}'_{rms}(z)$. For the regular flow, u'_{rms} is seen to increase near the bed as the flow accelerates in the positive direction, decay as the flow decelerates and increase again as the flow accelerates in the negative direction. Turbulence is generated close to the bed and propagates upwards, appearing increasingly later in time with height above the bed. The time-averaged turbulence intensity is maximum at approximately *z* = 0.38mm above the bed and decays with distance from the bed to near zero at z = ~100 mm. The velocity-skewness in the free-stream flow is reflected in higher turbulence intensity during the positive half-cycle compared with the negative half-cycle, as seen in the contour plot, and also in $u'_{rms}(t)$ at z = 0.38mm, which shows peak $u'_{rms}(t)$ of ~0.02m/s for the positive half-cycle and ~0.01m/s for the negative half-cycle.

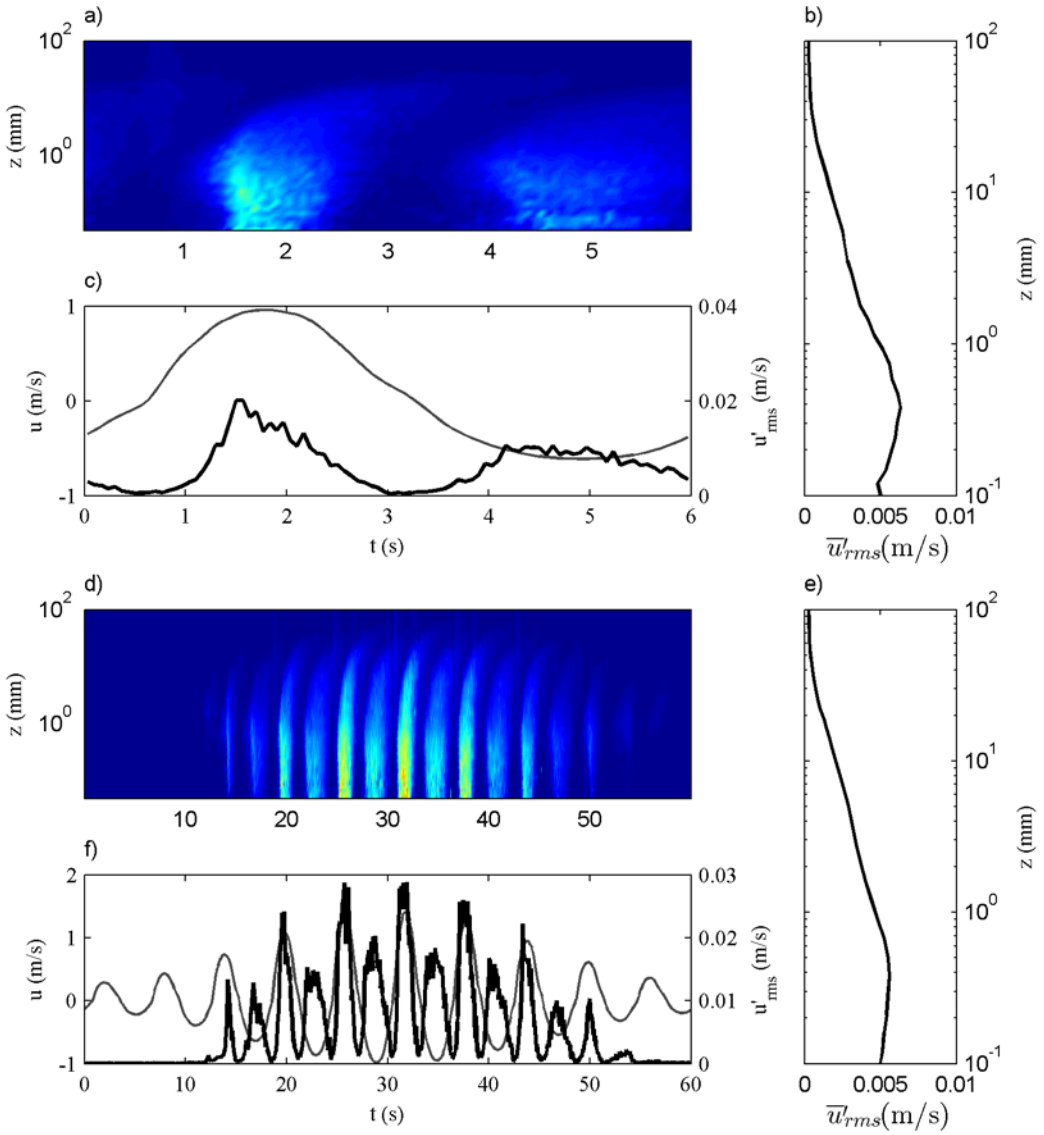

Figure 6. a) u'$_{rms}$(z,t) for CS-VR; b) t-averaged u'$_{rms}$(z); c) u'$_{rms}$(t) at z = 0.38 mm, corresponding to peak in t-averaged u'$_{rms}$(z), free-stream u(t) superimposed; d) to f) corresponding results for CS-VIS.

The turbulence intensity results for the corresponding irregular flow (VIS) echo the regular flow results. Again we see turbulence being generated near the bed and propagating upwards and we see the signature of the underlying velocity skewness, both in the contour plot and in the time-series. Peak u'_{rms} values are much higher for the irregular flow than for the regular flow because of the higher peak velocities, with maximum u'_{rms} being approximately twice that of the regular flow maximum. There is

good agreement between the regular and irregular flows in terms of $\overline{u'}_{rms}(z)$, with the maximum in each profile occurring at the same elevation (z = 0.38mm) and the profiles showing similar decay higher up. Also, looking at $u'_{rms}(t)$ at z = 0.38mm, there seems to be reasonably good correspondence in values of u'_{rms} for corresponding velocities between the regular and irregular flows, suggesting little effect of irregularity on the turbulence intensity at this level. Nevertheless, some effect of irregularity is evident in that intensity persists to later in the irregular group – compare $u'_{rms}(\mathrm{z} = 0.38\,\mathrm{mm}, t)$ for $0 \le \mathrm{t} \le 10$s and $50 \le \mathrm{t} \le 60$s. This effect is stronger higher up, especially at z ≈ 1mm (contour plots).

Figure 7 shows the corresponding results for the gravel-rough bed (note that the $u'_{rms}(\mathrm{z}, t)$ contour plots in Figures 6 and 7 have same scale). As expected, the increase in roughness results in higher turbulence generally, and an increase in height above the bed where $\overline{u'}_{rms}(z)$ is maximum (now at ~1.5mm). As for the sand-rough bed, the effect of the velocity skewness is evident in the contour plots and in $u'_{rms}(t)$ at z = ~1.5mm for the irregular flow (but not for the regular flow case, for which u'_{rms} appears to weaken somewhat at the time of peak positive velocity at z = ~1.5mm). There is good agreement between the $\overline{u'}_{rms}(z)$ profiles. Again, similar to what was observed in the case of the sand-rough bed, there is a build-up in turbulence intensity as the irregular flow group develops, leading to somewhat higher intensities during the decaying stage of the group compared with the developing stage.

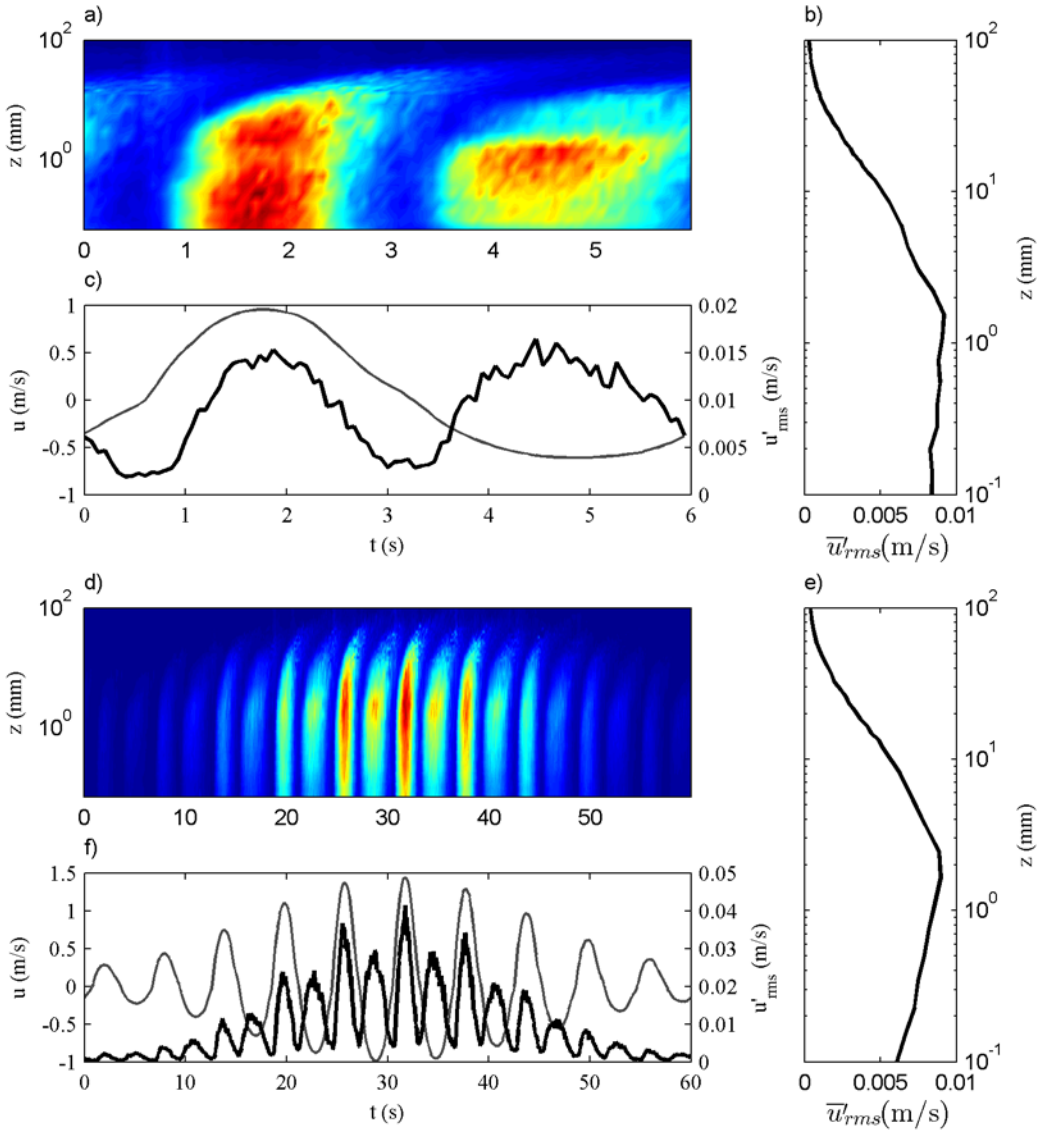

Figure 7. Similar to Figure 6 for cases GV-VR and GV-VIS respectively.

Figure 8 shows free-stream horizontal velocity, contour plots of $u'_{rms}(z,t)$ (different scale to that in Figures 6 and 7) and $u'_{rms}(t)$ at z corresponding to the peak in $\overline{u'}_{rms}(z)$ for three irregular velocity-skewed flows over the sand-rough bed: the sine-modulated flow VIS, (as in Figure 6), the backward-leaning-sawtooth flow VIB and the forward-leaning-sawtooth flow VIF. The contour plots and the time-series strongly reflect the corresponding free-stream flow, i.e. the peaks in u'_{rms} follow the peaks in the free-stream velocity, the overall shapes of the bottom time-series mirror the respective modulations. There is reasonable agreement between u'_{rms} peaks for corresponding peaks in free-stream velocity across the three flows, again suggesting little dependence of the turbulence on the cycle-to-cycle flow history in the near bed region. However, if no time-history effects were present then contour plots (e) and (h) would be mirror-images of each other, as would the time-series (f) and (i); this is not the case, suggesting that there may indeed be some time-history effect. The $\overline{u'}_{rms}(z)$ profiles for these flows (not shown) are similar in terms of shape and value and position of maximum $\overline{u'}_{rms}(z)$.

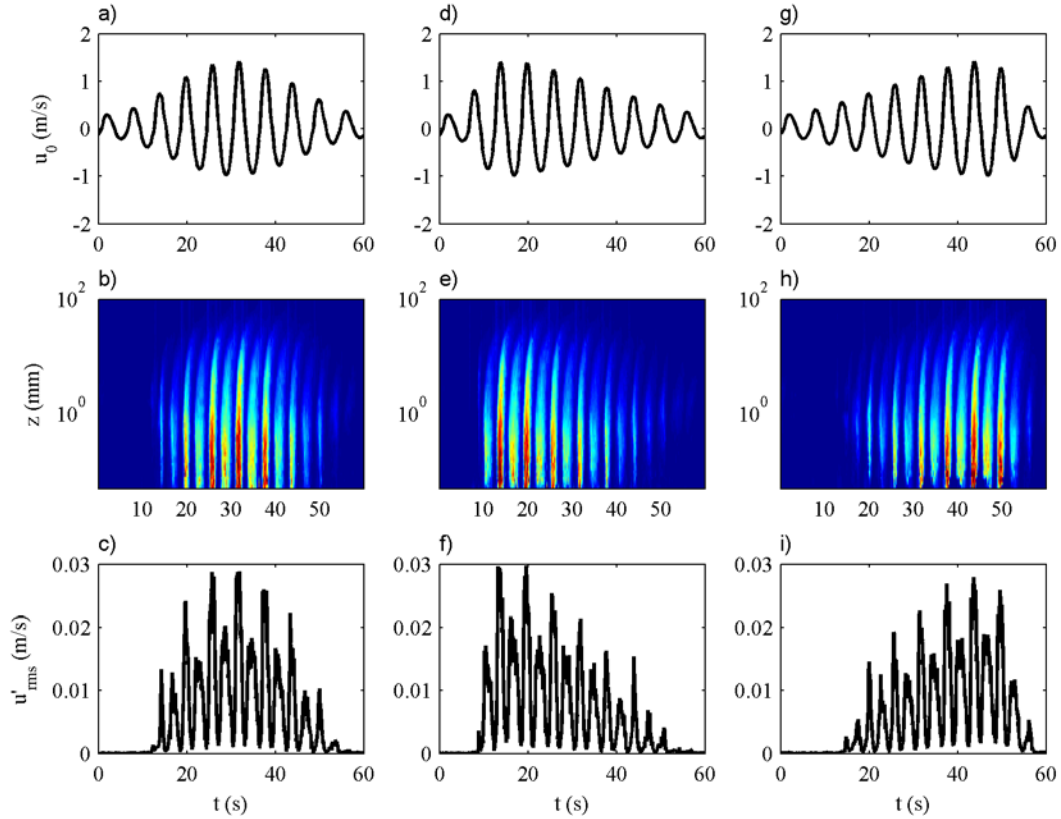

Figure 8. u'$_{rms}$ for cases CS-VIS (a-c), CS-VIF(d-f) and CS-VIB (g-i). Top row: Free-stream velocity. Middle row: contour plots of u'$_{rms}$(z,t). Bottom row: u'$_{rms}$(t) at z corresponding to peak t-averaged u'$_{rms}$(z).

Turbulent stress

Turbulent Reynolds stresses are calculated using

$$\overline{u'w'} = \sqrt{\sum_{i=1}^{N} \frac{TT(i)}{\sum TT}\left(u(i)-\tilde{u}\right)\left(\mathrm{w}(\mathrm{i})-\tilde{\mathrm{w}}\right)} \qquad (4)$$

Figure 9 shows example results for the Reynolds stresses for the sand-rough bed and the same three flows in Figure 8. Again we show the free-stream horizontal velocity, contour plots of the Re-stress and the time-series of Re-stress at elevation z corresponding to the peak in the vertical profile of the time-averaged Re-stress. Results for Re-stress tend to be noisier than for u'_{rms} because Re-stress involves the product of two fluctuating quantities and so more data/cycles are needed to obtain smooth transitions. Nevertheless the Re-stress results for each flow show reasonable consistency with the free-stream velocities: the peaks in Re-stress follow the peaks in free-stream velocity and the velocity skewness is evident in the Re-stress measurements.

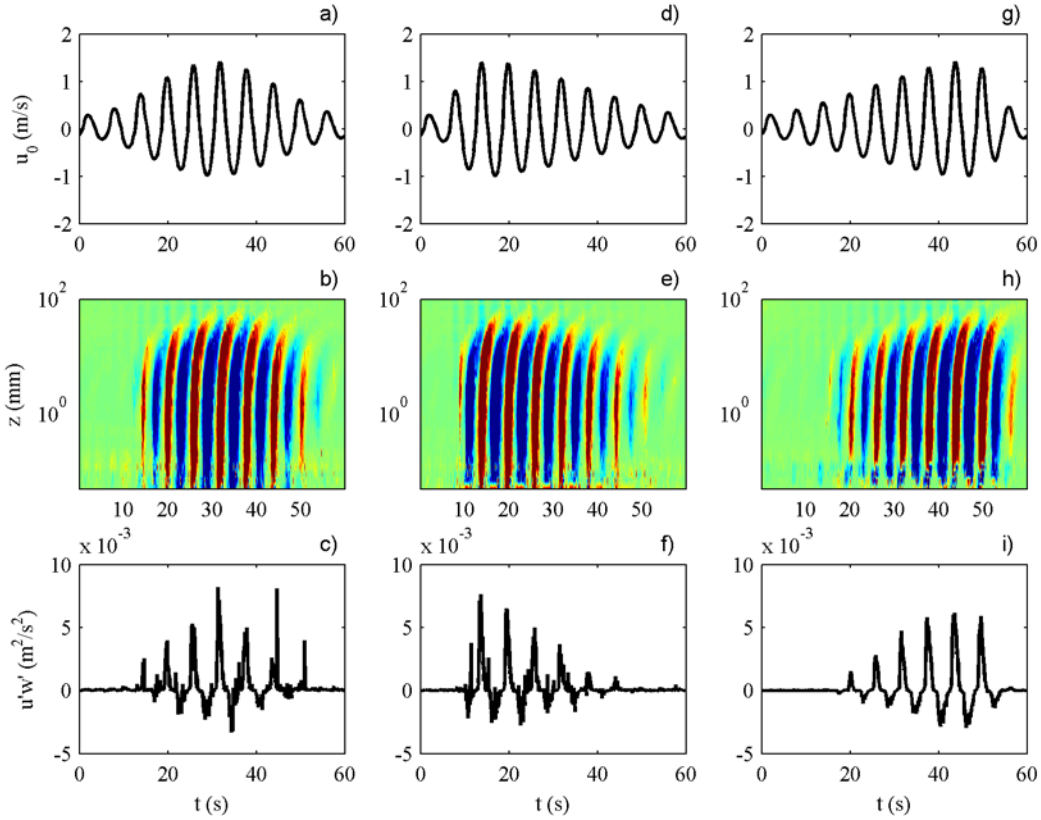

Figure 9. Similar to Figure 8 for Reynolds shear stress, $\overline{u'w'}$

Bed shear stress

Previous studies of oscillatory boundary layer flows have used log-law fitting to establish estimates of the bed shear stress (e.g. van der A, et al., 2011; Yuan and Madsen, 2014). There are complications in applying log-law to oscillatory flows because (i) the flow is not fully turbulent throughout the full half-cycle and (ii) it is not always clear to which part of the profile the log profile should be fitted (if at all). The log profile is given by

$$\frac{u(z)}{u_*} = \frac{1}{\kappa}\ln\frac{z}{z_0} \tag{5}$$

where $u_* = \sqrt{\tau_b / \rho}$ is the friction velocity, τ_b is bed shear stress, ρ is water density, κ = 0.4 is the von Karman constant and $z_0 = k_s / 30$, with k_s the roughness length. For the present analysis, we assume $k_s = 2.5d_{50}$ and determine the best-fit line containing a minimum of three data points (in addition to the intercept z_o) with correlation coefficient greater than 0.95.Example fits are shown in Figure 10 for the velocity-skewed regular flow over the sand-rough bed (case CS-VR). It was found that obtaining a fit was especially problematic during the positive half cycle (top 4 plots in Figure 10) because the velocity profile exhibits what looks like two log layers during this time. One layer is very close to bed, within the bottom 1-2mm; the second is higher up between approximately 1-2mm and 6-7mm. Using $z_0 = 2.5d_{50}/30$ favours the profile fitting the upper layer. For the negative half-cycle (bottom plots in Figure 10), there is better alignment between the “upper” and “lower” profiles

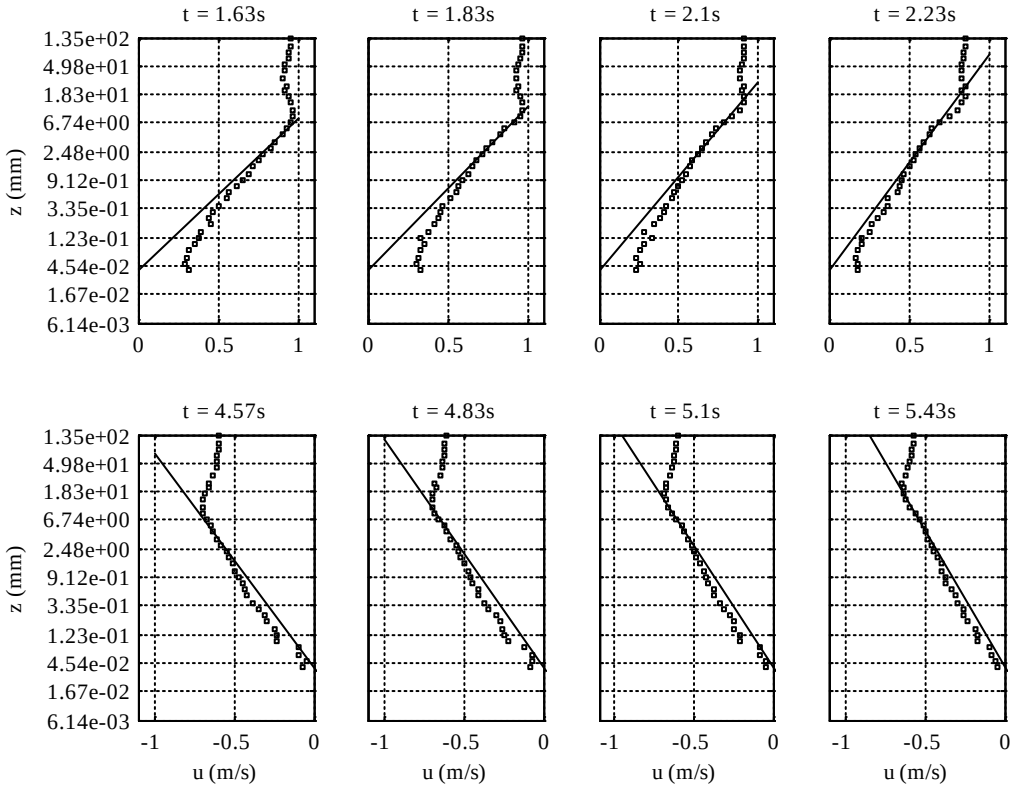

Figure 10. Example fits for log-law at various time instants for case CS-VR.

Log-law results for τ_b for the velocity-skewed regular flow over the sand-rough bed are shown in Figure 11. A log profile is not found during much of the accelerating phase in each half-cycle because the log profile is not fully developed. Successful fits are typically possible just before, or at the time of, peak flow velocity and throughout most of the decelerating phase. The velocity-skewness is clearly echoed in the bed shear stress estimates, with maximum positive half-cycle bed shear stress (~6Pa) approximately double that of the maximum negative half-cycle bed shear stress (~2.8Pa). Given that the maximum positive and maximum negative free-stream velocities are 0.96m/s and -0.61m/s respectively, the corresponding estimates of the friction factor $f_w = 2\tau_b / \rho \mathrm{U}^2$ are 0.013 and 0.015.

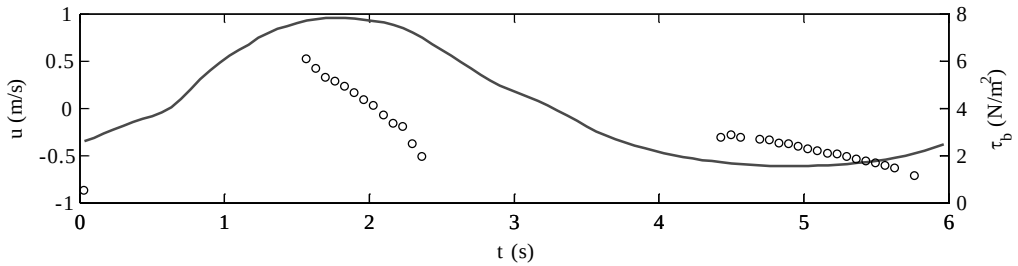

Figure 11. Free-stream velocity (line) and log-law-based bed shear stress (markers) for CS-VR.

Figure 12 presents τ_b estimates for the irregular flow VIS for both the sand-rough (top plot) and gravel-rough (middle plot) beds; also shown are the values of friction factor f_w corresponding to times of peak free-stream velocity. Note that log fits are not possible at the start and end of the group because of the very low velocities. The pattern of successful fitting close to the peak half-cycle velocity and for much of the decelerating phase is seen again here.

The results in Figure 12 for the irregular flow over the sand-rough bed (CS-VIS) are generally consistent with the results in Figure 11 for the corresponding regular flow. Again we see the underlying velocity skewness with maximum bed shear stress during positive half-cycles approximately twice

maximum bed shear stress during the negative half-cycles. The average of the friction factors for CS-VIS is 0.012, a little less than the 0.014 value for the corresponding regular flow CS-VR.

Bed shear stress estimates for the gravel-rough bed (GS-VIS) are much higher than for the sand-rough bed: the average of the friction factors is 0.03, 2.5 times that of the sand-rough bed. We note a tendency towards higher f_w at the early and late stages of the irregular group, consistent with lower relative roughness, a/k_s at these times. For the sand-rough and gravel-rough beds, there is little evidence of time-history effects within the bed shear stress estimates.

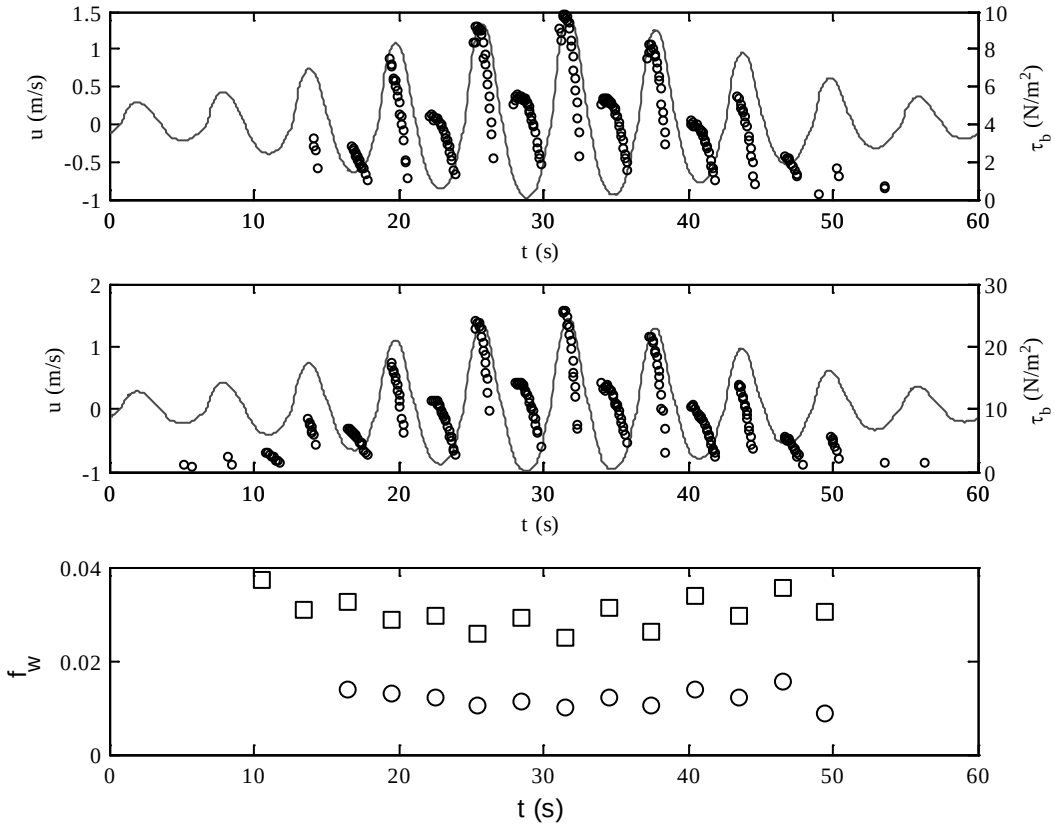

Figure 12. Log-law-based bed shear stress time-series for (top) CS-VIS and (middle) GV-VIS. Bottom plot: friction factor for CS-VIS (circles) and GV-VIS (squares)

CONCLUSION

New oscillatory flow tunnel experiments have been carried out to investigate boundary layer hydrodynamics for full-scale regular and irregular flows over sand-rough and gravel-rough fixed beds. The irregular flows were generated by amplitude modulation of regular flows, resulting in corresponding regular and irregular flows with the same T, u_{rms} and velocity and acceleration skewness. The approach therefore enables isolation of the effect of variation in flow velocity amplitude on the hydrodynamics, keeping all other key parameters constant. The velocity measurements within the boundary layer were obtained with high spatial resolution and with sampling rates in the 100s of Hz for most of the flow. The experiments cover a wide range of hydrodynamic conditions in terms of relative roughness and Reynolds number.

Example initial results, based on 1/15Hz phase-averaging, have been presented for the boundary layer development, turbulence intensity, turbulent stress and bed shear stress estimated from log-law fitting to instantaneous velocity profiles. In general, the results indicate that the hydrodynamics within a flow half-cycle are largely independent of the previous flow half-cycle, at least close to the bed where the presented results have focused. This means that the effects of irregularity on the hydrodynamics are weak (for the cycle period of 6s considered here). Time-history effects are not entirely absent however,

especially higher up from the bed. More detailed analysis, based on higher resolution phase-averaging, is ongoing with particular attention to turbulence at higher elevations above the bed.

ACKNOWLEDGMENTS

This research is part of the SINBAD project funded by EPSRC in the UK (EP/J00507X/1) and STW in The Netherlands (12058). Mahesa Bhawanin gratefully acknowledges receipt of a PhD Studentship from the University of Aberdeen.

REFERENCES

Jensen, B.L., Sumer, B.M. and J. Fredsøe. 1989. Turbulent oscillatory boundary layers at high Reynolds numbers, *J. Fluid Mechanics*, 206, 265-297.

Klopman, G. 1994. Vertical structure of the flow due to waves and currents. *H 840.3 (II)*, Delft Hydraulics.

Malarkey, J. and Davies, A.G. 2012. Free-stream velocity descriptions under waves with skewness and asymmetry. *Coastal Engineering*, 68, 78–95.

Sleath, J.F.A. 1987. Turbulent oscillatory flow over rough beds, *J. Fluid Mechanics*, 184, 349-409.

Tanaka, H. and Samad, M.A. 2006. Prediction of instantaneous bottom shear stress for smooth turbulent bottom boundary layers under irregular waves. *Journal of Hydraulic Research*, 44(1), 94–106.

van der A, D.A., O'Donoghue, T., Davies, A.G. and J.S. Ribberink. 2011. Experimental study of the turbulent boundary layer in acceleration-skewed oscillatory flow, *J. Fluid Mechanics*, 684, 251-283.

Yuan, J. and Madsen, O.S.. 2014. Experimental study of turbulent oscillatory boundary layers in an oscillating water tunnel, *Coastal Engineering*, 86, 63-84.